THE JOURNAL OF PHYSICAL CHEMISTRY C
Article
Cite This: J. Phys. Chem. C 2017, 121, 23249-23258
pubs.acs.org/JPCC

Influence of Thermal Annealing on Free Carrier Concentration in $(GaN)_{1-x}(ZnO)_x$ Semiconductors

Huafeng Huang,[†] Elizabeth C. Sklute,[‡] Keith A. Lehuta,[§] Kevin R. Kittilstved,[§] Timothy D. Glotch,[‡] Mingzhao Liu,[⊥] and Peter G. Khalifah*,[†,∥]

[†]Department of Chemistry, Stony Brook University, Stony Brook, New York 11794, United States
[‡]Department of Geosciences, Stony Brook University, Stony Brook, New York 11794, United States
[§]Department of Chemistry, University of Massachusetts Amherst, 710 North Pleasant Street, Amherst, Massachusetts 01003, United States
[∥]Chemistry Division, Brookhaven National Laboratories, Upton, New York 11973, United States
[⊥]Center for Functional Nanomaterials, Brookhaven National Laboratories, Upton, New York 11973, United States

Supporting Information

ABSTRACT: It was previously demonstrated that the efficiency of $(GaN)_{1-x}(ZnO)_x$ semiconductors for solar water splitting can be improved by thermal annealing, though the origin of this improvement was not resolved. In the present work, it is shown that annealing reduces the free carrier (electron) concentration of $(GaN)_{1-x}(ZnO)_x$. The time-, temperature-, and atmosphere-dependent changes were followed through two simple techniques: indirect diffuse reflectance measurements from 0.5 to 3.0 eV which show very high sensitivity to the free carrier response at the lowest energies and EPR measurements which directly probe the number of unpaired electrons. For the thermal annealing of investigated compositions, it is found that temperatures of 250 °C and below do not measurably change the free carrier concentration, a gradual reduction of the free carrier concentration occurs over a time period of many hours at 350 °C, and the complete elimination of free carriers happens within an hour at 550 °C. These changes are driven by an oxidative process which is effectively suppressed under actively reducing atmospheres (H_2, NH_3) but which can still occur under nominally inert gases (N_2, Ar). Surprisingly, it is found that the N_2 gas released during thermal oxidation of $(GaN)_{1-x}(ZnO)_x$ samples remains trapped within the solid matrix and is not expelled until temperatures of about 900 °C, a result directly confirmed through neutron pair-distribution fuction (PDF) measurements which show a new peak at the 1.1 Å bond length of molecular nitrogen after annealing. Preliminary comparative photoelectrochemical (PEC) measurements of the influence of free carrier concentration on photoactivity for water oxidation were carried out for a sample with $x = 0.64$. Samples annealed to eliminate free carriers exhibited no photoactivity for water oxidation, while a complex dependence on carrier concentration was observed for samples with intermediate free carrier concentrations. The methods demonstrated here provide an important approach for quantifying (and controlling) the carrier concentrations of semiconductors which are only available in the form of loose powders, as is commonly the case for oxynitride compounds.

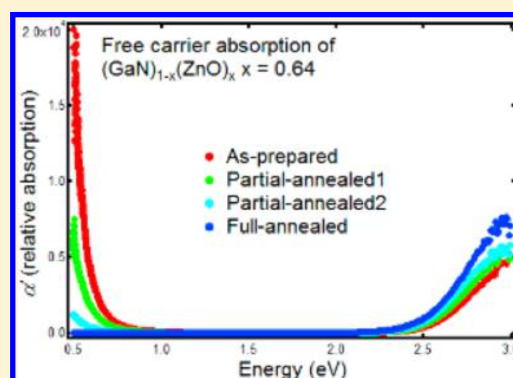

1. INTRODUCTION

The design and development of technologies for providing renewable energy solutions in a sustainable fashion is a pressing societal challenge.[1,2] Two of the most developed industrial solutions are photovoltaic- and wind-based energy generation technologies, though these approaches both suffer from the need for load leveling (due to their variable output) and the need for expensive connections to the electrical grid. An emerging technology which may avoid these limitations is the direct production of chemical fuels which can be stored and transported much more easily than the electrical energy. The most accessible pathway for solar fuel production is through solar water splitting, in which water molecules are split to produce H_2 fuel and O_2 gas as reaction products.[3] This can be accomplished using a semiconductor electrode which absorbs sunlight and uses the resulting photogenerated electrons and holes to drive the half-reactions for hydrogen and oxygen production, respectively.[4,5] While a wide variety of semiconductors capable of driving this process have been identified in the four decades since the initial pioneering work in this field, there is not yet an efficient and inexpensive semiconductor system for solar water splitting.

The highest reported efficiencies for overall water splitting carried out using suspended particles of a single-phase

Received: July 3, 2017
Revised: September 10, 2017
Published: September 13, 2017

ACS Publications © 2017 American Chemical Society

DOI: 10.1021/acs.jpcc.7b06455
J. Phys. Chem. C 2017, 121, 23249−23258

semiconductor which serves as both the photocathode and photoanode for overall water splitting were found for wurtzite-structured $(GaN)_{1-x}(ZnO)_x$ solid solution phases.[4] The maximum efficiencies for this system were observed not for as-synthesized semiconductors but for samples subjected to a postannealing treatment at 550 °C in air, a treatment which resulted in the external quantum efficiency of these semiconductors for overall water splitting being raised from 2.5 to 5.9%.[6,7] Given the relatively low treatment temperature and the absence of changes in X-ray diffraction patterns collected before and after annealing, it is expected that the enhanced activity was driven by changes in the free carrier concentration. However, in these preliminary studies, the carrier concentrations were not directly probed, so it is not known if the improved activity was the result of increased or decreased carrier concentrations. Furthermore, the fact that all measurements in this study were done on samples exposed to different annealing temperatures makes it difficult to assess which other thermally driven processes (such as sample degradation) might have mediated changes in activity.

It is generally expected that carrier concentration may greatly influence the photoelectrochemical performance of semiconductors. The photoelectrochemical activity measured for classical single crystal semiconductor photoanodes such as TiO_2[8,9] and $SrTiO_3$[10] was only observed after crystals were annealed under strongly reducing conditions to produce heavily n-doped samples with high electrical conductivities. While samples with smaller dimensions (such as thin films or suspended nanoscale powders) will be less likely to suffer from Ohmic losses associated with the sample resistance, it is still expected that the carrier concentration will strongly influence the minority carrier diffusion length and thus strongly influence the lifetime of photogenerated electrons and holes.[11,12] Since the internal quantum efficiency of a photoelectrochemical process is primarily determined by the relative rates of chemical reaction and charge-carrier recombination, the free carrier concentration is expected to greatly influence the efficiency of water splitting reactions.

For classic semiconductors such as Si and Ge, precise methods of for measuring and controlling the carrier concentration have been developed and deployed, and the behaviors of different dopants within these host lattices are well understood.[13,14] In contrast, information about effective dopants and free carrier concentration is completely lacking for many of the emerging complex semiconductors being considered for water splitting applications.[15] One reason for this is that these complex semiconductors have often only been studied in the form of polycrystalline powders rather than as single crystals or as crystalline films, and classical techniques for measuring carrier concentrations such as Hall effect measurements are poorly suited for use with powder samples of these resistive, large band gap semiconductors. It is therefore important to develop alternative methods for probing the carrier concentration in complex semiconductor systems.

In this work, new optical methods for probing the influence of annealing on the free carrier concentration of $(GaN)_{1-x}(ZnO)_x$ semiconductors are demonstrated. We have previously shown that $(GaN)_{1-x}(ZnO)_x$ powder samples exhibit a broad absorption feature well below their direct optical gap (2.5−3.4 eV, depending on x) in which the absorption rapidly increases with decreasing photon energy.[16] This absorption feature is ascribed to the interaction of light with free carriers based on its functional form (continually increases with decreasing energy, as is observed in other semiconductor systems[17−19]), and can be quantitatively fit to scaling relationships initially determined for single crystal samples of ZnO.[20] In the present work, optical spectroscopy is used to investigate the influence of annealing $(GaN)_{1-x}(ZnO)_x$ samples on their free carrier concentration. In particular, it is shown that bidirectional diffuse reflectance studies are very effective for measuring the optical response of powder samples down to energies of about 0.5 eV—a low energy range that is challenging to access in conventional integrating sphere measurements but which provides the clearest insights into free carriers. These optical measurements are complemented by physical and structural studies to investigate the chemical mechanism by which annealing may cause the free carrier concentration to be changed.

2. EXPERIMENTAL SECTION

$(GaN)_{1-x}(ZnO)_x$ semiconductor powders were synthesized using a modified layer double hydroxide (LDH) method described in detail elsewhere.[21] In order to investigate the effects of annealing, a single homogeneous sample of approximately 1 g mass was divided into four separate portions, one of which was not annealed and served as a control for measurements. The air annealing of synthesized $(GaN)_{1-x}(ZnO)_x$ samples was done in a box furnace at temperatures of 150−650 °C. For other atmospheres, samples were placed in a quartz boat cut from a 22 mm OD diameter quartz tube within a 25 mm OD diameter fused SiO_2 tube (GM Associates, Inc.). After an initial purge at a high gas flow rate, reactions were carried out under a continuous gas flow of 10 mL/min.

Laboratory X-ray diffraction (XRD) data of powdered samples annealed under a different atmosphere were collected on a Bruker D8 Advance laboratory diffractometer (Cu Kα λ = 1.54059 Å, 7−120° 2θ, 0.02 step size, 300 mm radius, 12 mm variable slits, 2.5° Soller slits, and a 192-channel Lynx-Eye 1D position sensitive Si detector). Time-of-flight neutron diffraction measurements were carried out on the Nanoscale-Ordered Materials Diffractometer (NOMAD) of the Spallation Neutron Source (SNS) at Oak Ridge National Laboratory, which has a total flight path of 21.5 m, utilizing a neutron beam collimated down to a diameter of about 6 mm. A typical data acquisition time of 45 min was used for each sample. Neutron powder diffraction data were reduced using a local software package developed for the NOMAD instrument. Structural lattice parameters were obtained from whole pattern fitting (Le Bail method) as implemented in the TOPAS software package (Bruker-AXS, version 4.2).

High energy optical data were collected with UV−vis diffuse reflectance spectroscopy on a PerkinElmer Lambda 950 spectrometer coupled with a 60 mm diameter integrating sphere. Powder samples were loaded into a cylindrical powder holder with a circular quartz window 16.60 mm in diameter and 1.50 mm thick. A scan range of 250−860 nm (1.44−4.97 eV with a lamp change at 319.20 nm) was used with a data interval of 1.30 nm and a scan rate of 182.25 nm/min. Calibration was done using a $BaSO_4$ (Alfa Aesar, 99.998%) 100% reflectance standard. Integrating sphere reflectance data were then transformed to a relative absorption spectrum using a Kubelka−Munk transform through the relationship of $\alpha'_{IS}(E) = (1 - R^2)/(2R)$, where R is the measured reflectance.[22]

Low energy optical data were collected on a bidirectional reflectance spectrometer using an 8° field of view (optic lens

DOI: 10.1021/acs.jpcc.7b06455
J. Phys. Chem. C 2017, 121, 23249−23258

coupled via an optical fiber to the detector) on an ASD Fieldspec3Max UV−vis-NIR spectrometer with a 512-element Si photodiode array detector for the 350−1000 nm energy range and two thermoelectric-cooled InGaAs photodiode detectors in the 1000−2500 nm range, giving a spectral resolution of 10 nm (at 1400 and 2100 nm) at low energies. The incident light was provided by an Ocean Optics HL-2000-HP tungsten halogen light source directed down a 600 mm Ocean Optics optical fiber. Data were collected with an incidence angle θ_i of 30° and an emission angle θ_e of 0° (angles specified relative to the normal of the sample plane). Incidence and emergence angles were set using a custom-built goniometer (estimated error <2°). All spectra were taken in the absence of ambient light and referenced to a calibrated Spectralon standard (Labsphere, Inc.) illuminated at the same angle as the sample. Reflectance data were taken at 10 scans per second by averaging 500 dark current scans, 500 white reflectance reference scans, and 500 sample reflectance scans. Powder samples were loaded into a black sample holder with a well depth of 5 mm and then leveled by tapping the sample holder. Bidirectional reflectance data were transformed to relative absorption spectra (α'_{BR}) using a transform derived by Hapke[23] (eqs 1−5):

$$\alpha'_{BR} = -\frac{1}{D}\ln\left(\frac{w - S_e}{1 - S_e - S_i + S_i w}\right) \quad (1)$$

$$w = 1 - \gamma^2 \quad (2)$$

$$\gamma(R) = \frac{[(\mu_0 + \mu)^2 R^2 + (1 + 4\mu_0\mu R)(1 - R)]^{1/2} - (\mu_0 + \mu)R}{1 + 4\mu_0\mu R} \quad (3)$$

$$S_i = 1.014 - \frac{4}{n(n + 1)^2} \quad (4)$$

and

$$S_e = \frac{(n - 1)^2}{(n + 1)^2} + 0.05 \quad (5)$$

In this Hapke transform, w is the single-scattering albedo which depends on the albedo factor γ. The experimental geometry is captured by μ_0 and μ, which are the cosines of the incidence angle θ_i and the emission angle θ_e, respectively. R is the measured bidirectional reflectance. S_e and S_i are external and internal scattering coefficients, which both depended on the refractive index n. When carrying out a Hapke transform, a single-valued sample refractive index, n, was refined so as to maximize the agreement between the relative absorbances inferred from bidirectional reflectance data (α'_{BR}) and through the Kubelka−Munk transform of integrating sphere data (α'_{IS}) over the energy range common to both instruments. Finally, D is the particle diameter. In the Hapke transform for the present samples, a common value of D = 1 μm was used for samples prepared with different compositions or under different reaction conditions in order to avoid adding scatter or bias into the relative absorbances, α'_{BR}, calculated for different samples.

Thermogravimetric analysis (TGA) data were collected using a Q5000 instrument (TA Instruments). About 10 mg of $(GaN)_{1-x}(ZnO)_x$ powder was placed in an alumina sample pan (100 μL volume). Samples were heated under a constant flow of air (25 mL/min), with a hold (2 h) at room temperature to allow complete gas exchange before ramping up in temperature. The sample temperature was raised at a ramp rate of 5 °C/min up to 350 °C, and held at that temperature for 24−96 h before ramping down to room temperature at the same rate.

Energy-dispersive X-ray spectroscopy (EDX) measurements of sample composition were carried out on a JEOL 7600F high-resolution scanning electron microscope (SEM). Sample powders were mounted using carbon tape attached to a 12.5 mm diameter aluminum stage, or alternatively, a suspension of the powder in ethanol was dispersed onto a 12.5 mm graphite stage (Ted Pella, Inc.).

X-band electron paramagnetic resonance (EPR) spectra were collected at room temperature with a Bruker Elexsys E-500 continuous wave spectrometer using the perpendicular mode of an ER-4116 dual-mode cavity with a quartz finger dewar insert used to fix the sample position. $(GaN)_{1-x}(ZnO)_x$ powders were loaded into a 4 mm outer diameter fused silica tube. Spectra were collected under identical sample conditions (sample position, sample amount, cavity quality factor, etc.) to allow integrated intensities to be compared between samples. EPR signals were fit with the first derivative of a single Lorentzian peak function where the central position, line width, and amplitude were fit variables. A linear background function was also added to account for the small slope and offset that was present even in the absence of free carrier signal.

A three-electrode photoelectrochemical (PEC) cell was constructed (Figure S1) and used on a measurement station equipped with a potentiostat (VersaStat 4, PAR) and a 150 W solar simulator with AM 1.5G filter (Newport-Oriel). $(GaN)_{1-x}(ZnO)_x$ powder suspensions were cast onto thin films using indium tin oxide (ITO) coated glass substrates with 1.5 cm × 1.5 cm dimensions (Thin Film Devices, Inc.), following a previously reported method[24] with final film dimensions of about 1.2 cm × 1.2 cm that were compatible with the illuminated spot size of 1.13 cm diameter. The functionalization of $(GaN)_{1-x}(ZnO)_x$ powders with RuO_2 water oxidation catalysts[25] was integrated into the film formation process. Enough $RuCl_3$ to produce a final loading of 5 wt % RuO_2 was dissolved in deionized water and stirred with $(GaN)_{1-x}(ZnO)_x$ powders. The suspension was then stirred and evaporated to dryness within a 50 mL alumina crucible. Immediately prior to casting films using a doctor blade technique (20 μm high blade, 5−10 mg/cm^2 sample loading), about 20 mg of $(GaN)_{1-x}(ZnO)_x$ was added to 80 μL of deionized water, mixed, and sonicated for 5 min. After casting the suspension onto ITO glass, the slide was annealed at 400 °C for 2 h to both oxidize $RuCl_3$ to form RuO_2 and to induce adhesion of $(GaN)_{1-x}(ZnO)_x$ particles to the slide. For the three-electrode PEC cell measurements, the counter electrode was Pt and the reference electrode was Ag/AgCl in 3 M KCl. The 0.5 M electrolyte of Na_2SO_4 was adjusted to a pH of 4.5 by adding H_2SO_4 prior to use following a previously optimized procedure.[26]

3. RESULTS AND DISCUSSION

3.1. Detection of Free Carrier Absorption. Most studies of the light absorption of semiconductor powders have focused on absorption properties near or above the semiconductor band gap. In contrast, the measurement of light absorption at energies well below the band gap has been generally neglected, in part due to the additional instrumentation challenges involved in collecting good data at energies below the bottom of the visible spectrum (<1.5 eV). In general, two detector

DOI: 10.1021/acs.jpcc.7b06455
J. Phys. Chem. C 2017, 121, 23249−23258

changes are typically needed to collect infrared absorption data between 0.5 and 1.5 eV. These detector changes commonly lead to significant discontinuities in the optical data due to the complex interplay of specular and diffuse scattering phenomena within the integrating sphere geometry routinely used for data collection.

We have recently been developing an alternative measurement strategy for studying the optical properties of semiconductors below their band gap using a bidirectional reflectance geometry. When this method is used, the contributions from specular reflectance can be readily minimized by choosing an incidence angle which significantly differs from the detector angle. The resulting aberrations induced by detector changes are small and can be easily corrected. However, the transformation of the raw integrating sphere reflectance data to a physically meaningful relative absorption spectrum, $\alpha'_{IS}(E)$, can no longer be accomplished through the simple Kubelka−Munk transform. More general mathematical relationships describing the angle-dependent diffuse reflectance of loose powders have been derived by Hapke, and in this work, a Hapke transform is utilized to obtain relative absorption spectra $\alpha'_{BR}(E)$ from bidirectional reflectance data over an energy range of 0.5−3.5 eV. This approach has enabled the collection of absorption data extending more than 2 eV below the band gap of $(GaN)_{1-x}(ZnO)_x$ semiconductors, enabling the first systematic study of below-gap absorption phenomena in this important family of visible-light-absorbing semiconductors.

Data in this energy range are particularly useful for probing the free carriers in this semiconductor system. In our previous published work on $(GaN)_{1-x}(ZnO)_x$ semiconductors, absorption data collected down to a minimum energy of 1.5 eV using integrating sphere methods were used to demonstrate that there is substantial below-gap absorption in this system that is an optical signature of the free carriers.[16] Over the energy range of 1.5−3.0 eV, this free carrier contribution was about 2 orders of magnitude weaker than that of the absorption associated with the band gap and could not be clearly seen unless the data were plotted in a manner to highlight this weak contribution.

In the present work, reflectance data were collected to a lower minimum energy of 0.5 eV in order to much more sensitively probe the free carriers, with a large improvement in sensitivity at lower energies occurring, since the free carrier absorption increases as inverse energy raised to the third power. At these low energies, the free carrier absorption may be comparable in magnitude to the absorption at energies above the band gap. Unconventional bidirectional reflectance spectroscopy techniques were used in order to more easily access lower energy data, and this work represents the first study of this type carried out for $(GaN)_{1-x}(ZnO)_x$ in the near-infrared portion of the electromagnetic spectrum. Samples for this work were prepared through a modified LDH synthesis technique that allowed an extended range of $(GaN)_{1-x}(ZnO)_x$ compositions to be accessed, most notably for the otherwise difficult to access Zn-rich side of the solid solution.

The relative absorption spectra, $\alpha'(E)$, for a series of $(GaN)_{1-x}(ZnO)_x$ semiconductors with x = 0.32−0.89 are shown in Figure 1. These spectra are a merged composite of low-energy bidirectional reflectance data (0.5−3.0 eV) and integrating sphere reflectance data (1.5−4.0 eV). Merging was accomplished by refining a single-valued refractive index, n, for each spectrum to minimize the difference α'_{BR} and α'_{IS} across the energies measured in both instruments (1.5−3.0 eV), as illustrated in Figure S2. Intriguingly, it can be seen that all $(GaN)_{1-x}(ZnO)_x$ compositions clearly exhibit strong absorption associated with free carriers scattered by ionized impurities[27−33] at energies below the band gap. In linearly scaled plots (top), it can be seen that the absorption associated with free carriers (at energies near 0.5 eV) may exceed the absorption associated with the semiconductor band gap (at energies above 3 eV). This illustrates the superb sensitivity of the low-energy infrared absorption response to semiconductor free carriers. The low-energy absorption monotonically increases with increasing Zn content. When the data are plotted on a logarithmic scale (bottom), it can be seen that this absorption changes by more than 2 orders of magnitude as the Zn cation fraction (x) is varied. This indicates that there is a very strong composition dependence of the free-carrier concentration for as-synthesized samples, and that the intrinsic dependence of $(GaN)_{1-x}(ZnO)_x$ semiconductor performance on composition cannot be effectively probed until a method for controlling the free carrier concentration is developed.

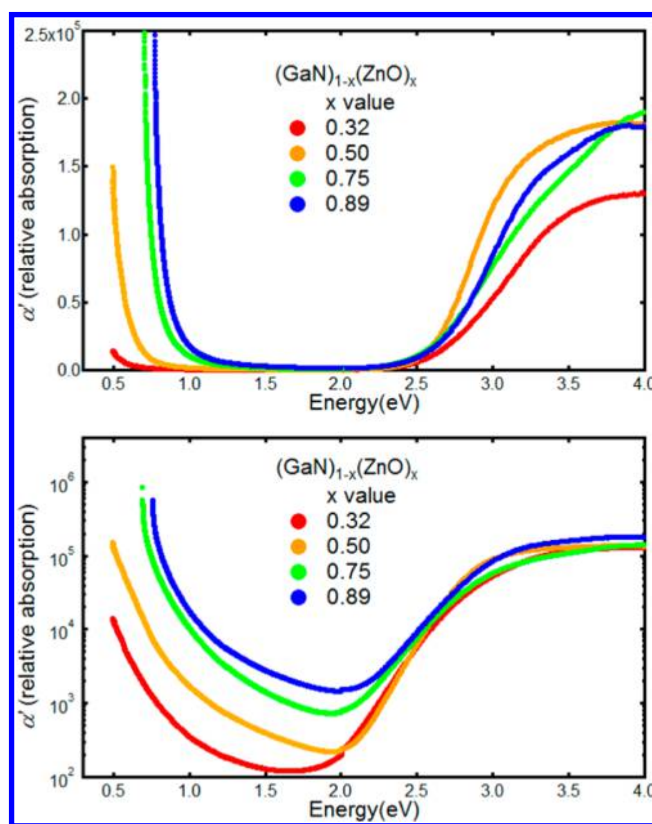

Figure 1. Relative absorption spectra of $(GaN)_{1-x}(ZnO)_x$ semiconductors plotted on a linear (top) and logarithmic (bottom) scale. Data below 2 eV were obtained from bidirectional reflectance measurements, while data above 2 eV were obtained from integrating sphere measurements through a Kubelka−Munk transform, which was used to set the scale of the vertical axis.

3.2. Thermal Annealing to Reduce Free Carrier Optical Response. Since infrared absorption has been demonstrated to provide a good signature of free carriers in powder samples of $(GaN)_{1-x}(ZnO)_x$ semiconductors, optical studies can potentially be used to quantitatively probe changes in the free carrier concentration induced by annealing. Prior studies of this system have shown that water splitting efficiency can be achieved through a postsynthesis anneal.[6] While it is expected that these thermal treatments improve performance

DOI: 10.1021/acs.jpcc.7b06455
J. Phys. Chem. C 2017, 121, 23249−23258

by changing the free carrier concentration, no efforts were made to directly study the carrier concentration in prior work. Furthermore, it should be noted that many methods used to functionalize $(GaN)_{1-x}(ZnO)_x$ semiconductors with water oxidation or hydrogen evolution cocatalysts include a processing step at elevated temperatures to promote the formation of the crystalline catalyst.[25,34−36] Any thermal processing step may drive a change in carrier concentration, whether or not this is an intended consequence.

A series of thermal annealing experiments were therefore designed and carried out to test what annealing temperatures, times, and atmosphere might strongly affect the free carrier concentration in $(GaN)_{1-x}(ZnO)_x$ semiconductors, using low-energy absorption spectra to provide feedback into potential changes. Initial tests were carried out using powders with a high Zn content of $x \sim 0.8$. As seen in Figure 2, thermal treatments

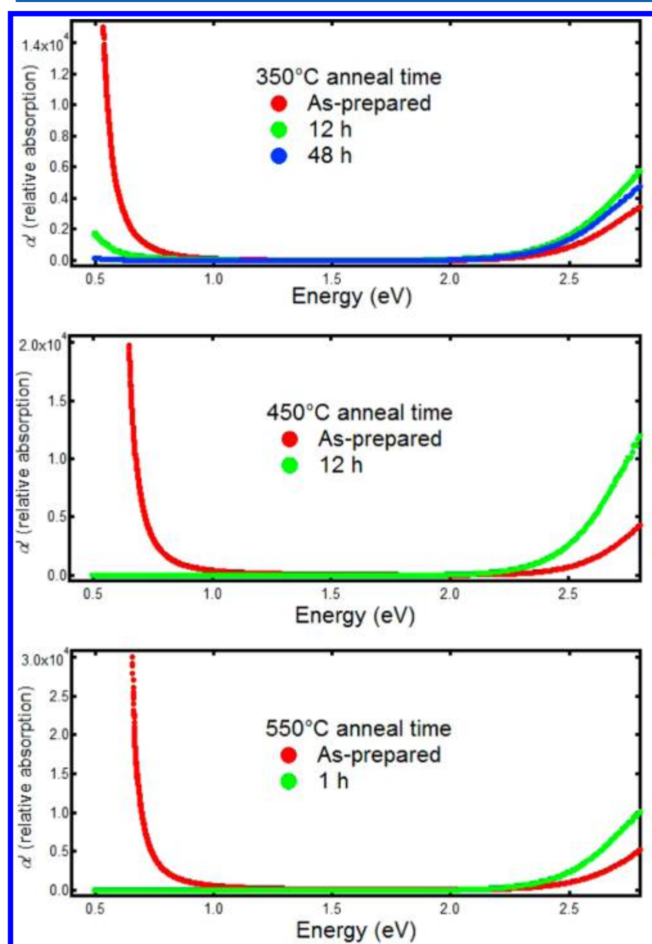

Figure 2. Relative absorption spectra, α'_{BR}, of $(GaN)_{1-x}(ZnO)_x$ with $x \sim 0.80$ obtained from bidirectional reflectance data collected before and after annealing in air at temperatures of 350−550 °C.

in air strongly influence the infrared absorption of these semiconductors. At temperatures of 550 °C and above, the free carrier absorption appears to be completely suppressed after a 1 h anneal. In contrast, an annealing temperature of 350 °C resulted in a gradual and nearly complete reduction of the infrared absorption over a time scale of 48 h. No observable changes in the absorption spectrum occurred when samples were annealed in air for 12 h at temperatures of 250 °C or below (Figure S3), suggesting that this is the lowest temperature which can be used to promote cocatalyst crystallization without affecting the semiconductor carrier concentration. The absorption data indicates that thermal treatments are an effective means of tuning the free carrier concentration in $(GaN)_{1-x}(ZnO)_x$ semiconductors.

The strong low-energy absorption in $(GaN)_{1-x}(ZnO)_x$ at energies of 1.5−2.0 eV has previously been described by an ionized impurity scattering model[16,28−33] in which the amplitude of this contribution to the overall absorption scales as λ^3. In this model, the amplitude of the absorption depends not just on the number of free carriers but also on the amount of ionized impurities present within the crystalline solid, thus greatly complicating the analysis. One method that is potentially capable of decoupling the contribution of free carriers and ionized impurities is EPR spectroscopy, which is directly sensitive to the spin associated with unpaired electrons. In addition, the Landé g-factor of a free carrier in a direct-gap semiconductor is specific to the host band structure and for ZnO the conduction band electron has $g = 1.96$.[20,37]

The EPR spectra for four fractions of one $(GaN)_{1-x}(ZnO)_x$ sample with $x \sim 0.65$ exposed to different annealing conditions are shown in Figure 3a. The amplitude of the EPR signal at $g = 1.96$ (3480 G) decreases with increasing annealing temperature and is indistinguishable from zero after annealing at 650 °C. This indicates the partial elimination of extrinsic free carriers at intermediate temperatures and their complete elimination after annealing at the highest temperature of 650 °C. The

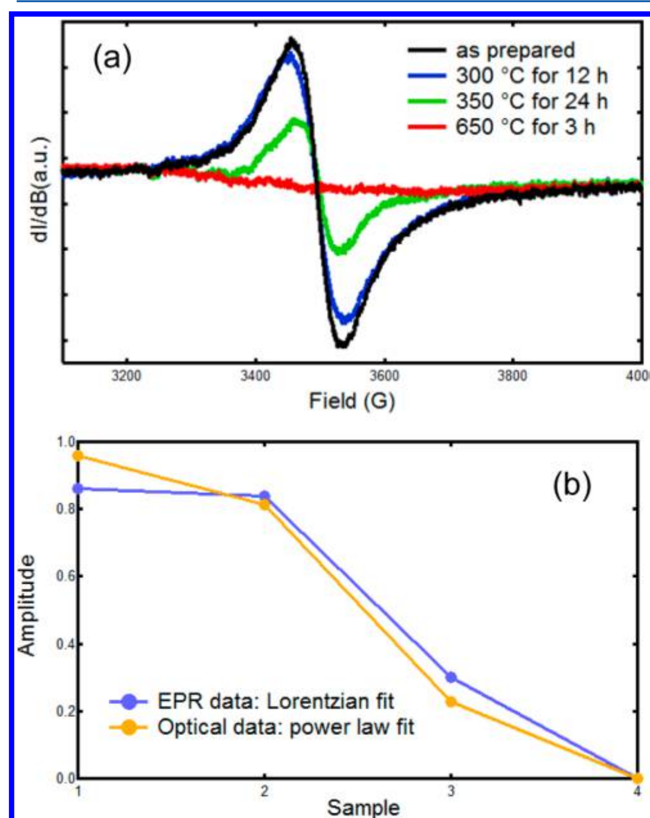

Figure 3. (a) Room temperature EPR spectra for as-prepared and annealed $(GaN)_{1-x}(ZnO)_x$ sample with $x = 0.65$. The spectra were normalized to a 9.60 GHz frequency. There is a systematic reduction in the intensity of the EPR signal with increasing temperature, and there is no detectable EPR signal after annealing at 650 °C in air. (b) Amplitudes of EPR data fitted to Lorentzian function and optical data fitted to power law were normalized together as a comparison.

DOI: 10.1021/acs.jpcc.7b06455
J. Phys. Chem. C 2017, 121, 23249−23258

normalized amplitude of the EPR signal was quantified using fits to a Lorentzian peak shape, and is compared to optical response in Figure 3b.

The amplitude of the low energy optical response of the same four samples over an energy range of 0.5−1.0 eV was determined by carrying out a global fit across the three samples with a detectable carrier concentration to a power law with a common power, which refined to 5.46. Although this functional form is not expected to reflect the true physical origin of the absorption processes (which are more likely due to a Drude response centered at zero frequency), it does allow the relative amplitudes of the optical response of these three samples to be compared on a common footing over a reasonably large energy window. When the relative amplitudes of the EPR and optical signals are linearly rescaled to fit on a common vertical axis (Figure 3b), it can be seen that there is excellent agreement between the two methods. This stands in contrast to the medium energy optical response from 1.4 to 2.3 eV previously attributed to ionized impurity scattering, which does not scale linearly with the EPR signal. In this system, the low energy 0.5−1.0 eV optical response appears to be directly proportional to the free carrier concentration, while the 1.4−2.3 eV optical response depends on both the free carrier and ionized impurity concentrations in a more complicated fashion. It is therefore concluded that the low energy optical absorption provides an effective means of quantifying the relative carrier concentrations of $(GaN)_{1-x}(ZnO)_x$ semiconductors using loose powder samples, and that this analysis method can likely be generally applied to other complex semiconductors being considered for solar water splitting applications.

3.3. Role of Oxidation. While it is clear that significant changes occur in $(GaN)_{1-x}(ZnO)_x$ semiconductors after annealing in air at elevated temperatures of 250−550 °C, the origin of these changes remains to be resolved. In two prior studies aimed at elucidating the sign of the charge carriers in $(GaN)_{1-x}(ZnO)_x$, the systems that were studied with $x = 0.30$ and $x = 0.05$−0.22 were found to be n-type semiconductors with electrons as majority carriers.[24,38] The origin of these excess electrons was not determined in these studies. In many semiconductors such as TiO_2 and $SrTiO_3$,[8−10] electron doping can be accomplished through the partial reduction of Ti^{4+} by exposure at high temperatures to strongly reducing conditions that lead to the loss of oxygen anions from the structural framework. However, neither Ga^{3+} nor Zn^{2+} cations in the $(GaN)_{1-x}(ZnO)_x$ semiconductors are redox-active ions. It is therefore expected that the carrier concentration is closely related to the defect chemistry associated with this wurtzite structure type, as is the case with the end member compounds of GaN and ZnO. It is not known whether defects associated with cation or anion sites are more likely, though we note that cation vacancies of up to a few percent have previously been proposed for Zn-poor $(GaN)_{1-x}(ZnO)_x$ semiconductors from studies separately quantifying the cation and anion fractions in this system.[16]

Thermogravimetric analysis (TGA) studies provide a good starting point for investigating the chemical changes that occur in $(GaN)_{1-x}(ZnO)_x$ semiconductors during heating. Figure 4 shows the mass changes that occur when a sample of $(GaN)_{1-x}(ZnO)_x$ with $x = 0.65$ is heated in an oxidizing atmosphere of air. During thermal oxidation, the sample mass should increase because every two N^{3-} anions will be replaced by three O^{2-} anions with the same net charge. The end point of this oxidation will be a mixture of ZnO and $GaZn_2O_4$. While

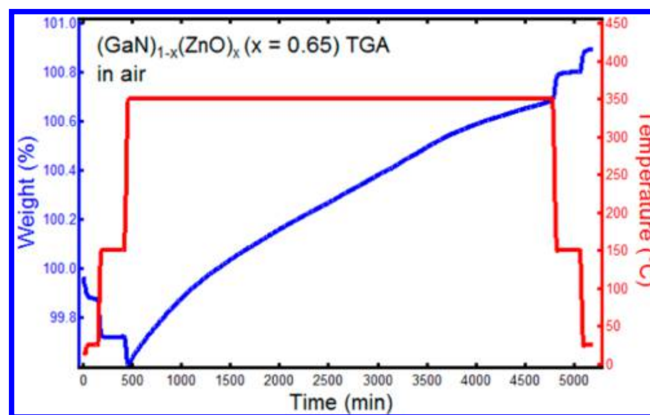

Figure 4. TGA data for a sample of $(GaN)_{1-x}(ZnO)_x$ with $x \sim 0.65$ heated in air up to a maximum temperature of 350 °C, and held there for about 3 days. The temperature profile is shown in red and the mass change in blue. The mass change corresponds to a sample decomposition rate of about 0.3%/h.

the complete oxidation of $(GaN)_{1-x}(ZnO)_x$ samples has been previously found to be best accomplished at temperatures of 800−900 °C,[16] it is clear from the present data that substantial partial oxidation can occur even at the relatively modest temperature of 350 °C. The mass increase of this sample over an ∼3 day hold at 350 °C (1.08%) is about one-quarter of that expected for the full oxidation of this sample (4.26%). The suppression of optical response at low energies during annealing in air at this temperature is likely driven by the slow oxidation of $(GaN)_{1-x}(ZnO)_x$ during this process.

In ceramic compounds, it is for the most part observed that high temperatures (>800 °C) are necessary to drive cation diffusion within solids, while anion diffusion is more facile and can often be accomplished at modest temperatures (>300 °C). The present TGA data suggest that the suppression mechanism of the free carrier absorption is due to the incorporation of O^{2-} anions provided by O_2 gas into the lattice. While the reduction of molecular O_2 may be primarily charge-balanced by the oxidation of lattice N^{3-} anions to N_2 gas, it is reasonable to expect that the same oxygen redox chemistry might also serve to oxidize the defects providing the n-type carriers seen in prior studies, thus neutralizing the excess electrons present in the as-prepared samples that contribute to the strong free carrier absorption at infrared energies. The oxidation mechanism can be generally summarized by the reaction $O_2(g) \rightarrow 2O^{2-}(s) + 4h^+$, which generates four holes in the solid state for each oxygen molecule that gets reduced into oxide anions.

Further insights into the role of redox chemistry can be obtained by annealing $(GaN)_{1-x}(ZnO)_x$ samples studied under other atmospheres. A comparison of the optical response of samples annealed under N_2, Ar, 5% H_2 (balance N_2), and NH_3 atmospheres is provided in Figure 5. The free carrier response is completely suppressed by annealing in N_2 and Ar. This suggests that even the small residual amounts of oxygen (1−100 ppm) present in these inert gases are sufficient to carry out the oxidative processes needed to remove free carriers. In contrast, no observable change is seen when the sample is annealed in flowing NH_3 gas at the relatively high temperature of 550 °C. NH_3 provides both an actively reducing environment for which the concentration of O_2 species is expected to be many orders of magnitude lower than for N_2 and Ar and reactive nitrogen species which can displace oxygen anions from a ceramic lattice. The relative importance of these two

DOI: 10.1021/acs.jpcc.7b06455
J. Phys. Chem. C 2017, 121, 23249−23258

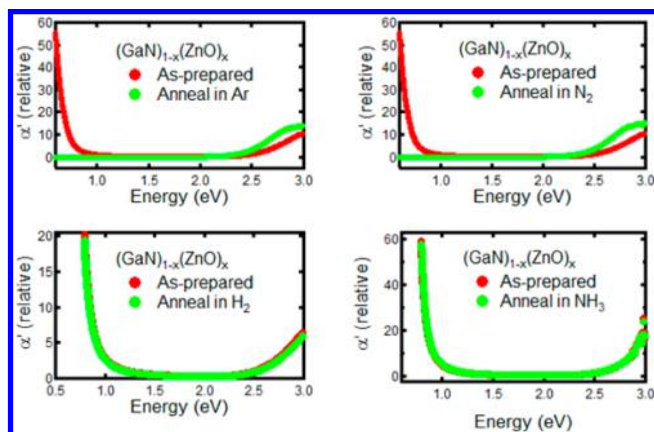

Figure 5. Relative absorption spectra of $(GaN)_{1-x}(ZnO)_x$ probing the changes in the optical response from free carriers after annealing in N_2, Ar, 5% H_2, and NH_3 atmospheres at temperatures of 550 °C (Ar, N_2) or 650 °C (NH_3, H_2). Red curves denote as-prepared $(GaN)_{1-x}(ZnO)_x$ samples and green curves the same sample after annealing. Due to sample availability, somewhat higher Zn content samples were used for samples annealed in H_2 and NH_3 (x = 0.95) than for anneals in Ar and N_2 (x = 0.83). Very high Zn content samples were used, as they had the highest initial free carrier concentration.

effects can be inferred by testing the effects of annealing under 5% H_2 at 550 °C as this gas provides a strongly reducing environment but no reactive nitrogen species. This H_2 anneal produces no observable change in the absorption spectrum, indicating that oxidation by O_2 is driving the suppression of the free carrier absorption, and that temperature alone does not change the free carrier concentration.

3.4. Influence of Annealing on Crystal Structure. Diffraction studies were used to determine if the annealing-induced changes substantially modify the bulk structure of $(GaN)_{1-x}(ZnO)_x$ semiconductors, or if annealing instead only impacts the defect chemistry of these compounds. Initial insights (Figure 6) were obtained by comparing the diffraction patterns of a sample with x = 0.83 annealed at 650 °C for 1 h under conditions for which the free carrier absorption was fully suppressed (atmosphere of air, N_2, or Ar). In all cases, it can be seen that there are no major changes in the peak position or intensity, and that there is no evidence for the formation of

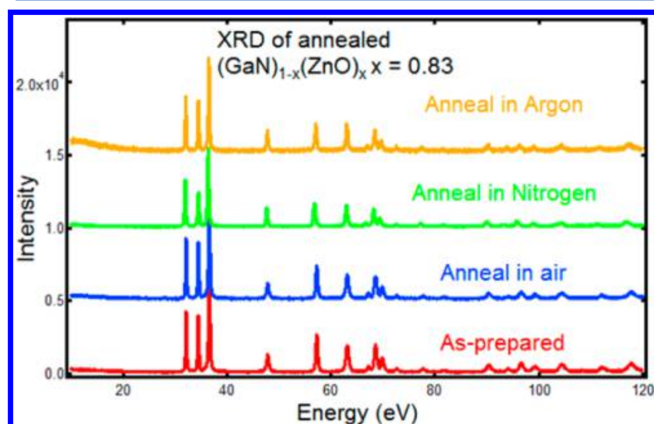

Figure 6. XRD patterns of $(GaN)_{1-x}(ZnO)_x$ sample with x = 0.83 and for the sample after three different annealing procedures (in air, N_2, or Ar at 650 °C for 1 h).

additional crystalline phases. The changes in the refined lattice parameters caused by annealing (Table S1) were in all cases less than 0.001 Å, and these changes were therefore not significant within the accuracy of this technique. Any structural changes in the crystalline phase are therefore expected to be minor, and are likely associated with defects.

A nontraditional diffraction technique that provides more direct insights into the compositional changes that occur on annealing is pair distribution function (PDF) analysis. Neutron PDF data for a $(GaN)_{1-x}(ZnO)_x$ sample with x = 0.64 annealed at different times are shown in Figure 7. It can be seen that the PDF spectrum remains qualitatively unchanged during annealing, though the magnitude of the PDF peaks decreases with increasing annealing time. The origin of this change can be inferred from an inspection of the low-r data in which a new peak centered at r = 1.08 Å appears after annealing. This very short bond distance is attributed to the presence of molecular nitrogen, for which the N≡N bond length is known to be 1.13 Å under standard conditions. At the temperature of the annealing treatments (250−650 °C), it is possible for O^{2-} anions to diffuse into the crystalline lattice to displace N^{3-} anions. However, the N_2 gas produced from this reaction lacks the mobility to diffuse out of the crystalline solid at these temperatures and this product gas will for the most part remain trapped in nonlattice physical voids within the solid. At higher temperatures where cations are mobile (> ∼750 °C), sintering of the solid can allow the physical voids to be eliminated, and a large drop in the sample mass is seen in TGA scans above this temperature (Figure S4) indicative of the loss of gaseous N_2 formerly in the voids. The presence of excess molecular N_2 trapped in the solid sample is conclusively supported by the magnitude of the mass gain during the thermal oxidation of $(GaN)_{1-x}(ZnO)_x$ phases, as the sample mass at intermediate temperatures is observed to far exceed the mass gain expected from the full replacement reaction ($2N^{3-} \rightarrow 3O^{2-}$). The present conclusion that N_2 gas is trapped in physical voids outside the lattice rather than in empty voids within the periodic lattice is opposite to the conclusions of some past studies on other oxynitrides[39−41] but is fully consistent with the lack of void space within the hexagonal close packed wurtzite lattice of $(GaN)_{1-x}(ZnO)_x$, and with the neutron PDF for this $(GaN)_{1-x}(ZnO)_x$ system which shows no evidence for new peaks associated with bonding of N_2 to the lattice despite the exceptionally strong scattering power of N nuclei (b = 9.36 fm) in neutron studies.

3.5. Photoelectrochemical Measurement. In addition to the spectroscopic probes of free carriers in $(GaN)_{1-x}(ZnO)_x$ systems, preliminary comparative photoelectrochemical (PEC) measurements of the influence of free carrier concentration on photoactivity for water oxidation were carried out using ITO-supported thin films of RuO_2-functionalized $(GaN)_{1-x}(ZnO)_x$ with x = 0.64 exposed to different annealing conditions using methods that have been previously developed.[24] This composition was selected, since it is expected to have a minimal band gap for the $(GaN)_{1-x}(ZnO)_x$ solid solution, leading to the strongest absorption of visible light. The photocurrent associated with water oxidation was tested by exposing these photoelectrodes to simulated AM1.5 sunlight under an applied bias of +0.5 V vs Ag/AgCl (+0.963 V vs RHE). The present measurements differ from earlier PEC studies of $(GaN)_{1-x}(ZnO)_x$ in two ways. First, previous PEC studies were only carried out for samples with lower Zn contents ($x \leq 0.42$). Second, prior PEC studies have

DOI: 10.1021/acs.jpcc.7b06455
J. Phys. Chem. C 2017, 121, 23249−23258

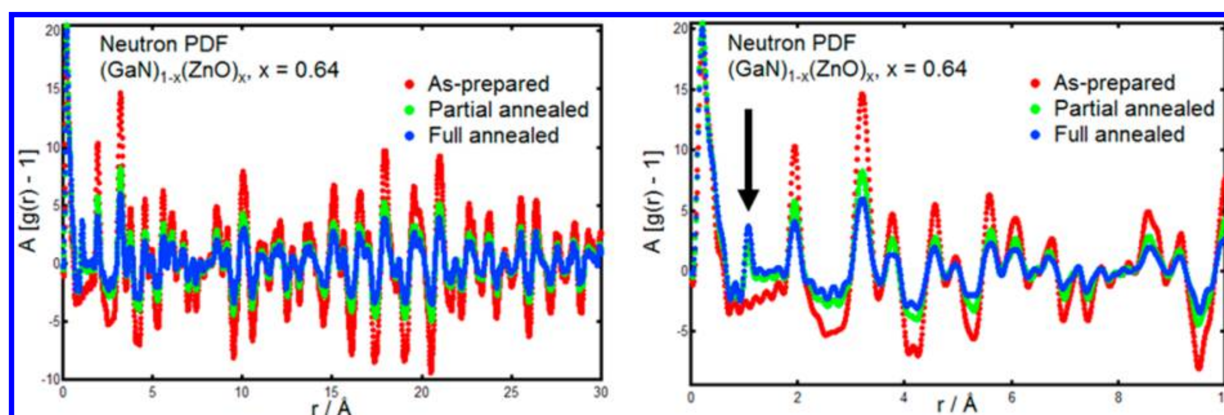

Figure 7. Comparison of neutron PDF data for a sample of $(GaN)_{1-x}(ZnO)_x$ with $x = 0.64$ prior to annealing (red), after partial annealing at 350 °C for 96 h (green), and after full annealing at 650 °C for 1 h (blue). Both the full spectrum (left) and a zoom of the low-r region (right) highlighting the molecular N_2 peak (black arrow) are shown.

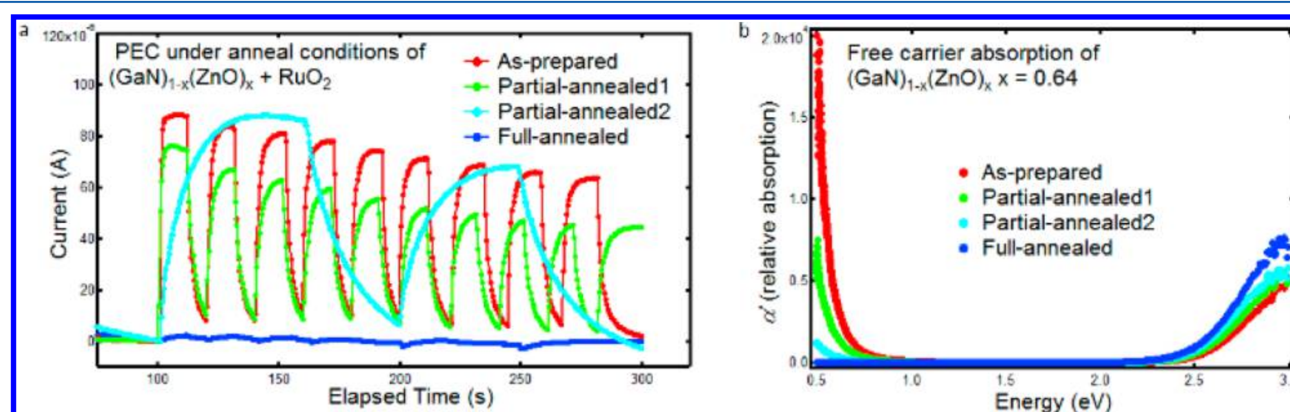

Figure 8. (a) PEC time trace of photocurrent produced under simulated AM 1.5 irradiation for RuO_2 (wt % = 5%) loaded $(GaN)_{1-x}(ZnO)_x$ electrode deposited on ITO glass with voltage 0.5 V vs Ag/AgCl applied in pH 4.5 Na_2SO_4 electrolyte. (b) Free carrier absorption of samples used in PEC tests of as-prepared $(GaN)_{1-x}(ZnO)_x$ with $x = 0.64$. "Partial-annealed1" sample was annealed at 350 °C for 24 h, while "partial-annealled2" sample was annealed at 350 °C for 96 h. "Full-annealed sample" was annealed at 650 °C for 1 h.

systematically explored the influence of Zn content but have not tested the influence of annealing on the photoactivity for water oxidation. It should also be noted that previous powder studies exploring the influence of annealing on photoactivity tested the rate of overall water splitting, rather than the rate of the water oxidation half-reaction which was measured in the present study.

For the specific sample of $(GaN)_{1-x}(ZnO)_x$ with $x = 0.64$, it was found that the photoactivity for water oxidation can be strongly modified by the annealing process (Figure 8a). The highest activity for the $x = 0.64$ was observed for the sample prior to annealing, with an initial photocurrent of about 0.1 mA/cm^2 under simulated sunlight. In contrast, annealing the same powder under conditions which fully suppressed the optical response (650 °C for 1 h) caused an almost complete suppression of the photoactivity. The same sample was also annealed under two different conditions which partially suppressed the free carrier optical response. The optical response was reduced by a factor of either 4 (350 °C for 24 h) or 10 (350 °C for 96 h), as seen in Figure 8b. For the former sample, a modest reduction in photoactivity of 10−25% was observed. For the latter sample, the maximum photocurrent was comparable to that of the pristine film, though with a much longer time constant for the rise and fall of the photoactivity. Complementary cyclic voltammetry and chronoamperometry data are provided in the Supporting Information (Figures S5 and S6).

The observed changes in photoactivity with annealing suggest that there is more than one mechanism by which the free carrier concentration influences the photoactivity. A reduction in the free carrier concentration is expected to increase the resistivity of the ceramic particles, which should have a detrimental effect on photoactivity. However, at low carrier concentrations, the lifetime of photogenerated carriers may greatly increase due to the reduced probability of recombination, thereby enhancing photoactivity—though the photoactivity may again decrease at very low carrier concentrations due to electronic transport limitations. An alternative origin for the longer time scale for the equilibration for the samples whose optical absorption was mostly suppressed is the contribution of low-lying defect states which are either completely filled or completely empty in other samples in this annealing series. The present preliminary data do not allow the validity of these hypotheses to be conclusively determined. However, a more comprehensive study of the photoactivity of $(GaN)_{1-x}(ZnO)_x$ semiconductor films exploring a wider range of annealing conditions and a wider range of Zn cation fractions produced using the methods demonstrated here should be effective in this regard.

3.6. Potential Origin of Free Carriers in $(GaN)_{1-x}(ZnO)_x$.

In the binary compound ZnO, some defect

DOI: 10.1021/acs.jpcc.7b06455
J. Phys. Chem. C 2017, 121, 23249−23258

mechanisms that give rise to free carriers are known. One is the presence of oxygen vacancies,[42] which can form under highly reducing conditions under which oxygen anions are oxidized to form molecular oxygen, causing a corresponding reduction of the lattice. A defect of this type could easily be compensated by annealing in the presence of oxygen, even at low oxygen partial pressures. Another known defect type in ZnO is interstitial Zn atoms.[20,37] These defects could be more difficult to compensate, as extra anions may need to be added to the structure to provide charge balance. During the oxidation of $(GaN)_{1-x}(ZnO)_x$ solid solution phases by oxygen, the net reaction involves replacing two N^{3-} anions with three O^{2-} anions. While this may normally be difficult to accomplish due to the lack of anion vacancies in the wurtzite lattice, extra Zn interstitial atoms may be able to combine with the extra anions, thereby expanding the net volume of the wurtzite phase.

It appears to be easier to form defects within the other binary end member GaN, as it is generally challenging to synthesize this phase in bulk without introducing charge carriers (most GaN powders are gray and not white). One known defect mechanism is the formation of cation vacancies, which can potentially be charge balanced through the partial replacement of N^{3-} by O^{2-} anions to produce gallium oxynitride phases,[43] and which have also been suggested to readily form for $(GaN)_{1-x}(ZnO)_x$ samples with low x values (or, equivalently, high Ga cation fractions).[16] The formation of cation defects in GaN has also been calculated to be energetically favorable under strongly reducing conditions even in the absence of oxygen.[44]

For the present solid solution samples, both the behavior during annealing and the sign of the anodic photocurrent suggest that the majority charge carriers are electrons and not holes for the $x = 0.64$ sample. This is consistent with the behavior previously seen in Hall measurements for single particles of $(GaN)_{1-x}(ZnO)_x$ semiconductors with lower Zn contents.[24,38] The facile reactivity with O_2 during thermal annealing at temperatures of 300 °C and above suggests that defect formation mechanisms driven by the loss of lattice O^{2-} or N^{3-} species as diatomic gases should also readily occur. These anion loss processes are expected to contribute extra electrons to the lattice and are fully consistent with the presence of n-type charge carriers inferred in data for solid solution samples.

Some possible spectroscopic insights into the nature of the defects producing charge carriers can potentially be obtained from an analysis of the g-values for $(GaN)_{1-x}(ZnO)_x$ samples obtained through EPR measurements with a suitable g-standard of 2,2-diphenyl-1-picrylhydrazyl (dpph). These g-values are provided in Table 1, with the spectra used for this analysis previously given in Figure 3a. It can be seen that the g-values increase with increasing Zn content, as might be expected on the basis of previously reported g-values for n-type GaN (g = 1.953)[45] and ZnO (g = 1.96).[37] This suggests that the origin for the n-type free carriers in the solid solution compounds is closely related to a mechanism present in the binary end members of GaN and ZnO. However, the exact nature of defects in the present sample cannot be directly determined from the present data, and follow-up experimental studies (e.g., photoluminescence) or theoretical studies provide a more effective means for conclusively identifying the nature of the defects that give rise to free carriers in $(GaN)_{1-x}(ZnO)_x$ samples.

Table 1. EPR-Measured g-Values for $(GaN)_{1-x}(ZnO)_x$

sample	g value
42% Zn	1.963
60% Zn	1.968
68% Zn	1.971
95% Zn	1.973
as prepared	1.972

4. CONCLUSIONS

It has been demonstrated that as-synthesized $(GaN)_{1-x}(ZnO)_x$ semiconductors prepared using modified LDH methods contain electrons as their free carriers. It is shown that the relative abundance of these free carriers can be quantified even for loose powder samples using EPR or low energy optical spectroscopy methods, with the latter approach having a particularly large dynamic range. These free carriers can be partially or completely eliminated by thermal annealing in the presence of molecular oxygen. This oxidative process produces N_2 gas as a byproduct, which is surprisingly trapped in nonlattice physical voids within the crystalline solid. The first photoelectrochemical tests on Zn-rich $(GaN)_{1-x}(ZnO)_x$ semiconductors with RuO_2 as a cocatalyst show that photoactivity for water oxidation depends on the carrier concentration but in a complex manner

■ ASSOCIATED CONTENT

Supporting Information

The Supporting Information is available free of charge on the ACS Publications website at DOI: 10.1021/acs.jpcc.7b06455.

Schematic of the PEC setup, self-referenced determination of n, absorption after low-temperature annealing, TGA response, cyclic voltammetry, chronoamperometry, and lattice parameters before and after annealing (PDF)

■ AUTHOR INFORMATION

Corresponding Author

*E-mail: kpete@bnl.gov.

ORCID

Kevin R. Kittilstved: 0000-0002-9852-7454
Mingzhao Liu: 0000-0002-0999-5214
Peter G. Khalifah: 0000-0002-2216-0377

Notes

The authors declare no competing financial interest.

■ ACKNOWLEDGMENTS

This work was primarily supported by DOE Grant No. DE-FG02-11ER16266 with the U.S. Department of Energy. Research carried out at Brookhaven National Laboratory was supported by the U.S. Department of Energy, Office of Basic Energy Sciences, under Contract No. DE-SC0012704. Research carried out in part at the Center for Functional Nanomaterials, Brookhaven National Laboratory, which is supported by the U.S. Department of Energy, Office of Basic Energy Sciences, under Contract No. DE-SC0012704. EPR spectra were collected at the University of Massachusetts Amherst EPR facility that was purchased with funds provided by the NSF (CHE-0443180).

DOI: 10.1021/acs.jpcc.7b06455
J. Phys. Chem. C 2017, 121, 23249−23258

REFERENCES

(1) Lewis, N. S.; Nocera, D. G. Powering the planet: Chemical challenges in solar energy utilization. *Proc. Natl. Acad. Sci. U. S. A.* **2006**, *103*, 15729.

(2) McKone, J. R.; Lewis, N. S.; Gray, H. B. Will solar-driven water-splitting devices see the light of day? *Chem. Mater.* **2014**, *26*, 407.

(3) Walter, M. G.; Warren, E. L.; Emily, L.; McKone, J. R.; Boettcher, S. W.; Mi, Q.; Santori, E. A.; Lewis, N. S. Solar water splitting cells. *Chem. Rev.* **2010**, *110*, 6446.

(4) Maeda, K.; Teramura, K.; Lu, D.; Takata, T.; Saito, N.; Inoue, Y.; Domen, K. Photocatalyst releasing hydrogen from water - Enhancing catalytic performance holds promise for hydrogen production by water splitting in sunlight. *Nature* **2006**, *440*, 295.

(5) Kasahara, A.; Nukumizu, K.; Hitoki, G.; Takata, T.; Kondo, J. N.; Hara, M.; Kobayashi, H.; Domen, K. Photoreactions on $LaTiO_2N$ under visible light irradiation. *J. Phys. Chem. A* **2002**, *106*, 6750.

(6) Maeda, K.; Teramura, K.; Domen, K. Effect of post-calcination on photocatalytic activity of $(Ga_{1-x}Zn_x)(N_{1-x}O_x)$ solid solution for overall water splitting under visible light. *J. Catal.* **2008**, *254*, 198.

(7) Maeda, K.; Domen, K. Photocatalytic water splitting: recent progress and future challenges. *J. Phys. Chem. Lett.* **2010**, *1*, 2655.

(8) Diwald, O.; Thompson, T. L.; Goralski, E. G.; Walck, S. D.; Yates, J. T. The effect of nitrogen ion implantation on the photoactivity of TiO_2 rutile single crystals. *J. Phys. Chem. B* **2004**, *108*, 52.

(9) Diwald, O.; Thompson, T. L.; Zubkov, T.; Goralski, E. G.; Walck, S. D.; Yates, J. T. Photochemical activity of nitrogen-doped rutile TiO_2 (110) in visible light. *J. Phys. Chem. B* **2004**, *108*, 6004.

(10) Miyauchi, M.; Takashio, M.; Tobimatsu, H. Photocatalytic activity of $SrTiO_3$ codoped with nitrogen and lanthanum under visible light illumination. *Langmuir* **2004**, *20*, 232.

(11) Casey, H. C., Jr; Miller, B. I.; Pinkas, E. Variation of minority-carrier diffusion length with carrier concentration in GaAs liquid-phase epitaxial layers. *J. Appl. Phys.* **1973**, *44*, 1281.

(12) Kumakura, K.; Makimoto, T.; Kobayashi, N.; Hashizume, T.; Fukui, T.; Hasegawa, H. Minority carrier diffusion length in GaN: Dislocation density and doping concentration dependence. *Appl. Phys. Lett.* **2005**, *86*, 052105.

(13) Fistul, V. I. *Heavily doped semiconductors*; Plenum Press: New York, 1969.

(14) Spitzer, W.; Fan, H. Y. Infrared absorption in n-type silicon. *Phys. Rev.* **1957**, *108*, 268.

(15) Osterloh, F. E. Inorganic materials as catalysts for photochemical splitting of water. *Chem. Mater.* **2008**, *20*, 35.

(16) Reinert, A. A.; Payne, C.; Wang, L. M.; Ciston, J.; Zhu, Y. M.; Khalifah, P. G. Synthesis and characterization of visible light absorbing (GaN)(1-x)(ZnO)(x) semiconductor nanorods. *Inorg. Chem.* **2013**, *52*, 8389−8398.

(17) Haga, E.; Kimura, H. Free-carrier infrared absorption in III-V semiconductors III. GaAs, InP, GaP and GaSb. *J. Phys. Soc. Jpn.* **1964**, *19*, 658.

(18) Spitzer, W. G.; Whelan, J. M. Infrared absorption and electron effective mass in n-type gallium arsenide. *Phys. Rev.* **1959**, *114*, 59.

(19) Schroder, D. K.; Thomas, N. R.; Swartz, J. C. Free carrier absorption in silicon. *IEEE J. Solid-State Circuits* **1978**, *13*, 180.

(20) Kittilstved, K. R.; Schwartz, D. A.; Tuan, A. C.; Heald, S. M.; Chambers, S. A.; Gamelin, D. R. Direct kinetic correlation of carriers and ferromagnetism in Co^{2+}: ZnO. *Phys. Rev. Lett.* **2006**, *97*, 037203.

(21) Huang, H.; Reinert, A. A.; Khalifah, P. G. To be published.

(22) Kubelka, P.; Munk, F. A contribution to the optics of pigments. *Z. Tech. Phys.* **1931**, *12*, 593.

(23) Hapke, B. *Theory of reflectance and emittance spectroscopy*; Cambridge University Press: New York, 2012.

(24) Hashiguchi, H.; Maeda, K.; Abe, R.; Ishikawa, A.; Kubota, J.; Domen, K. Photoresponse of GaN: ZnO electrode on FTO under visible light irradiation. *Bull. Chem. Soc. Jpn.* **2009**, *82*, 401.

(25) Maeda, K.; Teramura, K.; Takata, T.; Hara, M.; Saito, N.; Toda, K.; Inoue, Y.; Kobayashi, H.; Domen, K. Overall water splitting on $(Ga_{1-x}Zn_x)(N_{1-x}O_x)$ solid solution photocatalyst: Relationship between physical properties and photocatalytic activity. *J. Phys. Chem. B* **2005**, *109*, 20504.

(26) Maeda, K.; Teramura, K.; Masuda, H.; Takata, T.; Saito, N.; Inoue, Y.; Domen, K. Efficient overall water splitting under visible-light irradiation on $(Ga_{1-x}Zn_x)(N_{1-x}O_x)$ dispersed with Rh-Cr mixed-oxide nanoparticles: Effect of reaction conditions on photocatalytic activity. *J. Phys. Chem. B* **2006**, *110*, 13107.

(27) Han, W.; Zhang, Y.; Nam, C.; Black, C. T.; Mendez, E. E. Growth and electronic properties of GaN/ZnO solid solution nanowires. *Appl. Phys. Lett.* **2010**, *97*, 083108.

(28) Visvanathan, S. Free carrier absorption arising from impurities in semiconductors. *Phys. Rev.* **1960**, *120*, 379.

(29) Fan, H. Y. Infra-red absorption in semiconductors. *Rep. Prog. Phys.* **1956**, *19*, 107.

(30) Fan, H. Y.; Spitzer, W.; Collins, R. J. Infrared absorption in n-type germanium. *Phys. Rev.* **1956**, *101*, 566.

(31) Thomas, D. G. Infrared absorption in zinc oxide crystals. *J. Phys. Chem. Solids* **1959**, *10*, 47.

(32) Weiher, R. L. Optical properties of free electrons in ZnO. *Phys. Rev.* **1966**, *152*, 736.

(33) Chattopadhyay, D.; Queisser, H. J. Electron scattering by ionized impurities in semiconductors. *Rev. Mod. Phys.* **1981**, *53*, 745.

(34) Xiong, A.; Yoshinaga, T.; Ikeda, T.; Takashima, M.; Hisatomi, T.; Maeda, K.; Setoyama, T.; Teranishi, T.; Domen, K. Effect of hydrogen and oxygen evolution cocatalysts on photocatalytic activity of GaN: ZnO. *Eur. J. Inorg. Chem.* **2014**, *2014*, 767.

(35) Maeda, K.; Teramura, K.; Lu, D.; Saito, N.; Inoue, Y.; Domen, K. Noble-metal/Cr_2O_3 core/shell nanoparticles as a cocatalyst for photocatalytic overall water splitting. *Angew. Chem.* **2006**, *118*, 7970.

(36) Maeda, K.; Ohno, T.; Domen, K. A copper and chromium based nanoparticulate oxide as a noble-metal-free cocatalyst for photocatalytic water splitting. *Chemical Science* **2011**, *2*, 1362.

(37) Halliburton, L. E.; Giles, N. C.; Garces, N. Y.; Luo, M.; Xu, C.; Bai, L.; Boatner, L. A. Production of native donors in ZnO by annealing at high temperature in Zn vapor. *Appl. Phys. Lett.* **2005**, *87*, 172108.

(38) Han, W. Growth and electronic properties of GaN/ZnO solid solution nanowires. *Appl. Phys. Lett.* **2010**, *97*, 083108.

(39) Le Gendre, L.; Marchand, R.; Piriou, B. Raman scattering investigations of dinitrogen entities in oxidized $LaTiO_2N$ perovskite. *Eur. J. Solid State Inorg. Chem.* **1997**, *34*, 973−982.

(40) Aguiar, R.; Logvinovich, D.; Weidenkaff, A.; Reller, A.; Ebbinghaus, S. G. Thermal oxidation of oxynitride perovskites in different atmospheres. *Thermochim. Acta* **2008**, *471*, 55−60.

(41) Mi, Q.; Ping, Y.; Li, Y.; Cao, B.; Brunschwig, B. S.; Khalifah, P. G.; Galli, G. A.; Gray, H. B.; Lewis, N. S. Thermally stable N_2-intercalated WO_3 photoanodes for water oxidation. *J. Am. Chem. Soc.* **2012**, *134*, 18318−18324.

(42) Vanheusden, K.; Seager, C. H.; Warren, W. T.; Tallant, D. R.; Voigt, J. A. Correlation between photoluminescence and oxygen vacancies in ZnO phosphors. *Appl. Phys. Lett.* **1996**, *68*, 403.

(43) Kikkawa, S.; Nagasaka, K.; Takeda, T.; Bailey, M.; Sakurai, T.; Miyamoto, Y. Preparation and lithium doping of gallium oxynitride by ammonia nitridation via a citrate precursor route. *J. Solid State Chem.* **2007**, *180*, 1984.

(44) Neugebauer, J.; Van de Walle, C. G. Atomic geometry and electronic structure of native defects in GaN. *Phys. Rev. B: Condens. Matter Mater. Phys.* **1994**, *50*, 8067.

(45) Fanciulli, M.; Lei, T.; Moustakas, T. D. Conduction-electron spin resonance in zinc-blende GaN thin films. *Phys. Rev. B: Condens. Matter Mater. Phys.* **1993**, *48*, 15144.

DOI: 10.1021/acs.jpcc.7b06455
J. Phys. Chem. C 2017, 121, 23249−23258